Boletim da Sociedade Astronômica Brasileira, **31**, no. 1, 154-157

Can globular clusters contain dark matter?

Oswaldo D. Miranda, Carolina Gribel, & José Williams Vilas-Boas

[1] Instituto Nacional de Pesquisas Espaciais — INPE
e-mail: oswaldo.miranda@inpe.br, carol.gribel@gmail.com, williams.boas@inpe.br

Abstract. In a recent work, Gribel et al. (2017) proposed a unified scenario describing both the cosmological star formation, from redshift 20 up to the present, and the local (Galactic) star formation. In particular, the consistency between these two star forming rates shows that most of the star formation occurs in dark matter minihalos with typical masses $\sim 10^6$ to $10^9 M_\odot$. In these structures, the stars are more concentrated, while the dark matter extends beyond the stellar distribution encompassing the star forming regions – this kind of structure resembles globular clusters. In the present work, we discuss the consistency of this unified scenario with the observational data of star forming regions.

Resumo. Em recente trabalho, Gribel et al. (2017) propuseram um cenário unificado descrevendo tanto a formação estelar cosmológica, no intervalo de deslocamento para o vermelho de 20 até o presente, quanto a formaçao estelar local (ou Galáctica). A consistência entre estas duas taxas de formação estelar mostra que a maior parte das estrelas se forma em minihalos de matéria escura com massas típicas $\sim 10^6$ a $10^9 M_\odot$. Nestas estruturas, as estrelas estão mais concentradas, enquanto a matéria escura estende-se além da distribuição estelar englobando as estrelas formadas – este tipo de estrutura assemelha-se a aglomerados globulares. Neste trabalho, discutimos a consistência deste cenário unificado a partir de dados associados com regiões de formação estelar.

Keywords. Cosmology: theory – large-scale structure of Universe – Galaxies: halos – Galaxies: star formation – globular clusters: general

1. Introduction

The formation of globular clusters (GCs) is a fascinating mystery in astrophysics (Freeman 2017). All the works discussed over the last 50 years in the literature can be grouped into four different possibilities to explain the formation of GCs. The first proposal made by Peebles & Dicke (1968) evokes the formation of GCs before the formation of the galaxies themselves. Thus, the formation of the GCs should have occurred at high redshifts in an environment with low metallicity. In this scenario, it would be natural for GCs to be formed within the first dark matter halos, which probably began to decouple from the expansion of the universe at redshifts $\sim 20-30$. Several works over the years have followed this scenario through different modifications (see, for example, Fall & Rees 1985; Katz & Ricotti 2014).

The second proposal suggests that the formation of GCs occurred in wet mergers. In this case, GCs formed in the early universe in a metal-poor environment. After, at intermediate redshifts, a new generation of GCs are formed from a metal-rich environment. In this proposal, there will be a bimodality in the distribution of GCs. That is, two different populations in terms of age-metallicity will be formed in the universe (see, for example, Ashman & Zepf 1992; Schweizer 1987).

The third proposal, which is known in the literature as multiphase collapse, was originally proposed by Forbes et al. (1987). It considers that GCs form during the collapse of proto-galaxies at intermediate redshifts. A second step starts when the formation of the galactic discs makes the interstellar medium dense enough to resume the formation of globulars. Similar to the previous proposal, this produces a bimodality in the distribution of the GCs. However, this effect arises in intermediary redshifts contrary to the previous proposal whose first phase occurs before the formation of the proto-galaxies.

The last proposal considers in situ formation (see, Armandroff & Zinn 1988; Côté et al. 1998). In this scenario, there will also be a bimodality in the distribution of GCs. Those metal-poor will form in the halos of galaxies while metal-enriched GCs will form in galactic bulges. It is possible to verify, from the four scenarios above, that regardless of the particular choice there is a common denominator between these scenarios. That is, the formation of GCs is intrinsically connected with the very formation of the large-scale structures of the universe.

Since the large-scale structures of the universe originate from the evolution of perturbations in dark matter, it is natural, at least in principle, to suppose that GCs may have originally been formed within structures similar to dark matter minihalos. As there are several GCs in the Milky Way, the question we intend to evaluate in this work is whether it would be possible to describe the formation of systems similar to GCs from the evolution of the large-scale structures of the universe. Certainly, to advance in this direction it is necessary to have a model that allows treating in a consistent way both the cosmological star formation and the Galactic star formation. Perhaps from a unified model of star formation, it is possible to obtain some clues to answer the question proposed in the title of this work.

Recently Gribel et al. (2017) tried to go in that direction, proposing a model that unifies the descriptions of the cosmological and Galactic star formation rates. In particular, their model permits to describe the cosmological star formation from redshift 20 up to the present, while at the same time it allows describing the star formation of the Galaxy. The result is an interesting unified scenario showing: the role of the supersonic turbulence in the formation of the large-scale cosmological structures, the origin of the so-called Larson's law for the star formation of the Galaxy (which happens to be a natural consequence of the formation of the large-scale structures of the universe) and brings as an additional result the formation of systems similar to GCs embedded in dark matter minihalos. It is this last result, a possibility of globular clusters embedded in dark matter halos, which we intend to explore in this work.

This paper is organized as follows: in Section 2, we review the model of Gribel et al. (2017). In Section 3, we present our re-

sults, and we present a summary and our conclusions in Section 4.

2. The unified scenario for star formation

The model developed by Gribel et al. (2017) starts from the *ansatz* that there is a perfect mapping between the cosmic star formation rate (CSFR) and the local rate of star formation (SFR). This can be represented by the equation

$$\frac{\dot{\rho}_\star(z)}{\langle\varepsilon\rangle} = \dot{\rho}_{\rm SFR} = \frac{\rho_{\rm g}}{\tau_{\rm s}} \int_{s_{\rm crit}}^{\infty} \exp\left(\frac{3}{2}s\right) p_{\rm hk}(s) ds, \tag{1}$$

where $\dot{\rho}_\star(z)$ is the CSFR, $\langle\varepsilon\rangle$ is the efficiency for star formation (a function of the redshift), $\rho_{\rm g}$ is the gas density at $z = 0$, $\tau_{\rm s}$ is the timescale for star formation ($\sim$ 2Gyr).

The integral represents the SFR, in particular, describing the so-called 'multi-freefall model'. The function $p_{\rm hk}(s)$ describes the probability distribution function used by Hopkins (2013) to study the density fluctuations induced in the clouds (local SFR) by the turbulence (see, for details, Gribel et al. 2017). The s parameter is related to the gas density used for star formation through $s \equiv \ln(\rho_{\rm g}/\rho_0)$, while $s_{\rm crit}$ considers that there should be a minimum density contrast in the molecular clouds for star formation to begin.

As discussed by Hopkins (2013), the function $p_{\rm hk}(s)$ is considerably good when compared to data on a large Mach number range, and variance in numerical simulations related to Galactic star formation. Its functional form is given by

$$p_{\rm hk}(s) = I_1\left(2\sqrt{\lambda\omega(s)}\right) \exp\left[-(\lambda+\omega(s))\right] \sqrt{\frac{\lambda}{\theta^2\omega(s)}}$$

$$\lambda \equiv \frac{\sigma^2_{\rm s,V}}{2\theta^2}; \quad \omega(s) \equiv \frac{\lambda}{(1+\theta)} - \frac{s}{\theta} \quad (\omega(s) \geq 0), \tag{2}$$

where $I_1(x)$ is the modified Bessel function of the first kind, $\sigma_{\rm s,V}$ is the volume-weighted standard deviation of the logarithmic density fluctuations, and θ is the intermittency parameter. In the zero-intermittency limit ($\theta \to 0$), Equation (2) takes the form of a lognormal distribution.

In order to obtain the SFR from non-isothermal PDF (Equation 2), it is necessary to adequately characterize $\sigma_{\rm s,V}$. To do this, we use the Rankine-Hugoniot conditions to obtain the following equation for the density contrast $x \equiv \rho_{\rm g}/\rho_0$

$$x^\Gamma + \Gamma b^2 \mathcal{M}^2 \left(\frac{1}{x} - 1\right) - 1 = 0, \tag{3}$$

where Γ is the polytropic index.

Solving the transcendental Equation (3), we obtain the variable $s = \ln(\rho_{\rm g}/\rho_0)$ and its logarithmic density variance, which is given by

$$\sigma^2_{\rm s} \simeq \ln\left(1 + \frac{\rho_{\rm g}}{\rho_0}\right), \tag{4}$$

where for $\Gamma = 1$, the non-trivial solution of Equation (3) yields $x \equiv \rho_{\rm g}/\rho_0 = b^2\mathcal{M}^2$.

The connection between $\sigma_{\rm s,V}$ and $\sigma_{\rm s}$ is made through the intermittency parameter (θ), which in turn is related to Γ ($\Gamma \neq 1$) by a power law. That is

$$\theta = 0.035 b \mathcal{M} \Gamma^{-2}, \tag{5}$$

which in turn produces

$$\sigma^2_{\rm s,V} = \sigma^2_{\rm s}\,(1+\theta)^{3/2}. \tag{6}$$

Once the set of previous equations is solved consistently, it becomes possible to produce a mapping that connects the left side of equation (1), which describes the CSFR, to the right side of this equation describing the SFR (Galactic star formation). Figures 1 and 2 show the mapping of the CSFR made through the SFR. See that on the left side of equation (1) we find the 'cosmology'. Thus, the values of the parameters $\dot{\rho}_\star$ and $\langle\varepsilon\rangle$ vary with redshift as described in Gribel et al. (2017). On the right side of the equation, the gas density is fixed with its value at redshift $z = 0$. Thus, the value of the integral must be adjusted to reproduce the variations of the parameters dependent on the redshift. For consistency, at $z = 0$ the integral must be equal to 1. The numerical exploration of the integral is searched for the value for the Mach number that maintains the equality of this equation. The procedure is repeated for each redshift value of the CSFR, enabling the Mach number to keep equation (1) always satisfied. As can be seen in the figures, the mapping is perfect between the two star-formation rates.

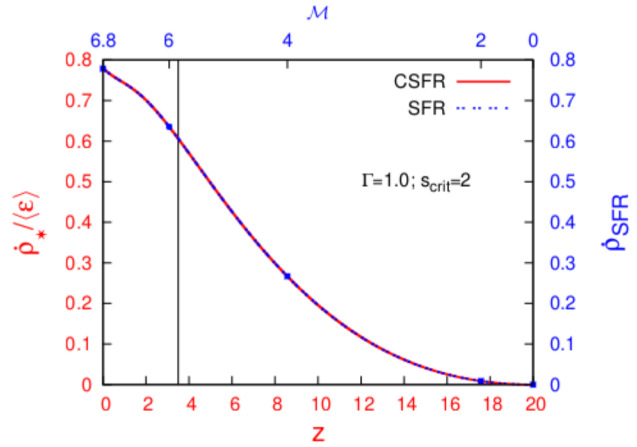

Figure 1. The solution of the Equation (1) with $s_{\rm crit} = 2$ and polytropic index $\Gamma = 1$. The evolution of the CSFR, weighted by the average efficiency, as a function of the redshift, is presented in the $y1 - x1$ axes (in red). The axes $y2 - x2$ (blue) show the SFR obtained with the frozen value of $\rho_{\rm g}$ at $z = 0$, and looking for the value of the Mach number that satisfies the equality of this equation (see Gribel et al. 2017 for details).

Since it is possible to have a unifying scenario describing the two star formation rates, as shown in Figures 1 and 2, one can analyze the consequences and implications intrinsically associated with this unification. The main conclusions drawn by Gribel et al. (2017) are:

- At high redshifts ($z \sim 20$), begins the conversion of baryonic matter to form stars. The baryonic matter falls into the gravitational potential of the dark halos. In this phase, the gas presents low Mach numbers (subsonic scale $\mathcal{M} \sim 0.5$).
- As redshift decreases, halos with greater mass are formed. The density of both the gas and the stars increases, causing the degree of gas turbulence parameterized by $\mathcal{M}$ to increase as well.
- The turbulence shows a dual feature, inducing the star formation with high values of $\langle\varepsilon\rangle$, until reaching a certain $\mathcal{M}_{\rm crit}$ (see Gribel et al. 2017). For $\mathcal{M} > \mathcal{M}_{\rm crit}$, a strong decrease in the efficiency of star formation occurs.

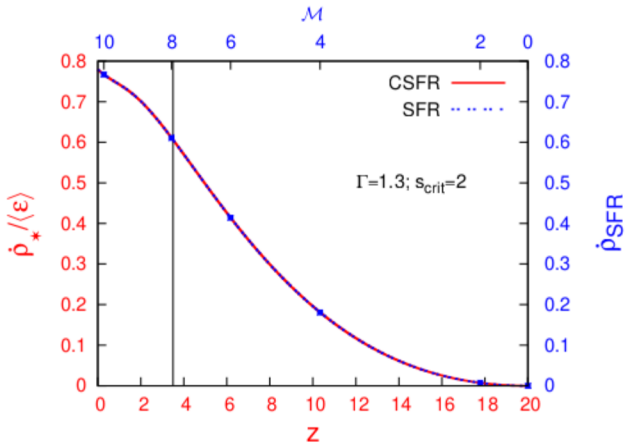

Figure 2. Similar to Figure 1 but with the polytropic index $\Gamma = 1.3$.

• Using the CSFR as a map for the SFR, we find a relation for the velocity dispersion of the gas that is directly involved with the star formation within the dark matter halos. This relationship is similar to that obtained by Larson in 1981 (see Larson 1981). It associates the internal motions with the structure of the molecular clouds where the star formation takes place, being known in the literature as Larson's law.

• The formulation that allowed Gribel et al. (2017) to obtain Larson's law implicitly suggests that the halos of greater mass are composed of a number of halos with much smaller masses. Therefore, the star formation at high redshifts would be processed, in part, in structures similar to globular clusters.

3. Dark matter in globular clusters

Since the cosmological star formation is tied to the formation of the large-scale structures of the universe, it is natural that the baryonic matter that forms stars will be concentrated in the innermost regions of the dark matter halos. On the other hand, gas not converted to stars will distribute more diffusely inside the halos. Looking now from the side of the local star formation, one can use the specific formalism of the Galactic star formation to obtain relations involving physical parameters such as gas velocity and temperature in the cosmological star-forming regions. As the size of the cosmological structures increases over time, it becomes possible to identify the relationship involving the gas mass converted into stars with the characteristic size scale where the star formation processes. In particular, Gribel et al. (2017) proposed that

$$\langle R_\star(z)\rangle = \frac{\rho_\star}{\rho_g}\langle R_V(z)\rangle, \tag{7}$$

where ρ_g is the total gas entering the halos and being distributed in the virial radius ($\langle R_V(z)\rangle$) of these structures. As before, $\rho_\star$ is the density of stars formed in the halos. Thus, $\langle R_\star(z)\rangle$ represents the characteristic size of the star formation regions.

The functional form of equation (7) clearly shows that the star formation processes inside dark matter halos. Thus, the stars are enveloped by a distribution of non-baryonic matter contained in $\langle R_V(z)\rangle$ and characterized by the total dark mass $\langle M_{DM}\rangle$. Note that the virial radius is defined when the dark matter density contrast is ~ 200. Thus, the dark mass contained into $\langle R_V(z)\rangle$ is

$$\langle R_V(z)\rangle = \left(\frac{3\,\langle M_{DM}\rangle}{800\pi\rho_B(z)}\right)^{1/3}, \tag{8}$$

where $\rho_B(z)$ is the background density (dark matter component) at redshift z.

On the other hand, following Hennebelle & Chabrier (2008, 2009), we can write for the gas velocity dispersion

$$\langle V_{rms}^2\rangle = \mathcal{M}^2 c_s^2, \tag{9}$$

where c_s represents the thermal sound speed.

Considering a polytropic equation of state and that the gas behaves as a perfect gas, we obtain

$$P = \kappa\rho_{mol}^\Gamma = \frac{k_B}{\mu m_H}\rho_{mol}T(\rho_{mol}), \tag{10}$$

producing

$$\kappa = \frac{k_B}{\mu m_H}\rho_{mol}^{1-\Gamma}T(\rho_{mol}), \tag{11}$$

where ρ_{mol} is the star-forming gas that lies in the innermost part of the halos. The corresponding equation for the temperature of the gas becomes

$$T(\rho_{mol}) = T_0\left(\frac{\rho_0}{\rho_{mol}}\right)^{1-\Gamma}, \tag{12}$$

and the thermal sound speed can be written as

$$c_s = \sqrt{\frac{\partial P}{\partial\rho_{mol}}} = \left(\Gamma\frac{k_B}{\mu m_H}\rho_0^{1-\Gamma}T_0\right)^{1/2}\rho_{mol}^{(\Gamma-1)/2}, \tag{13}$$

where k_B is the constant of Boltzmann, m_H is the mass of the hydrogen atom, $\mu \sim 0.5$ is the average molecular weight of the gas, and ρ_0 and T_0 correspond to the average values for the gas density and temperature, respectively.

The estimate for the value of ρ_0 can be obtained from $s = \ln(\rho_g/\rho_0)$. Assuming that, within $\langle R_V\rangle$, the gas has a typical density contrast of the order of s_{crit} ($\langle s\rangle \simeq s_{crit}$), then one can express ρ_0 as a function of ρ_g and as a function of ρ_{mol}.

Now, defining the value of the characteristic temperature, T_0, we can estimate the thermal sound speed as a function of the redshift. As we have the solution $\mathcal{M}$ versus z, then one can calculate $\langle V_{rms}\rangle$ in Equation (9). Once ρ_{mol} is converted to $\rho_\star$ on the scale $\langle R_\star\rangle$, the solution $\langle V_{rms}\rangle$ versus $\langle R_\star\rangle$ can be determined.

The Figures (3) and (4) show the result of this analysis. The observational data indicated in these Figures were obtained from the survey of Heyer et al. (2001). The original catalog corresponds to 10,156 molecular clouds, and we selected 5,400 spectra whose peaks in temperature are higher than 3.5K[1].

Once we have selected the molecular clouds, we binned the data determining median and error (as indicated in the Figures). The blue and red lines present two different results of our model (dependence with Γ and T_0). It is possible to verify that our model, within 2σ, reproduces very well the V_{rms} versus $R_\star$ data of the Heyer et al. (2001) molecular cloud catalog in the range $0.1 - 30$ pc.

When Larson developed his work in the 1980s (see Larson 1981), he obtained a relation between $\langle V_{rms}\rangle$ and $\langle R_\star\rangle$ of the type

$$\langle V_{rms}\rangle = V_0\left(\frac{\langle R_\star\rangle}{1\text{pc}}\right)^\eta, \tag{14}$$

[1] The choice of line temperatures greater than 3.5K is a criterion to obtain an optimal signal-to-noise ratio in the CO spectra. For these clouds, this will probably correspond to kinetic temperatures $T_0 \sim 10 - 20$ K.

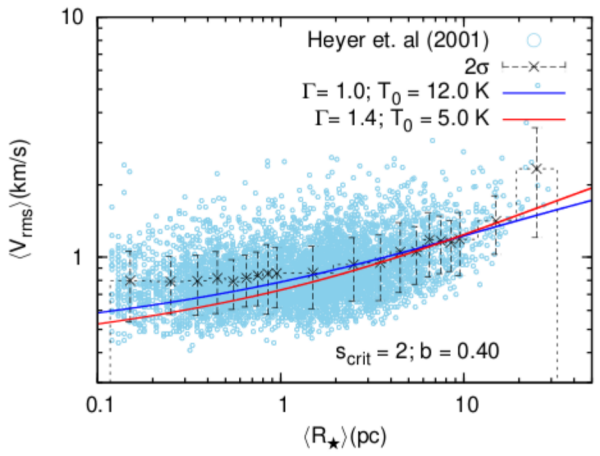

Figure 3. Observational data of molecular clouds from Heyer et al. (2001) catalog. The data were binned and were determined mean and median as indicated in the Figure. The blue and red lines indicate two different solutions of our model for different values of Γ and T_0. As shown, there is good fit of the model to the data within 2σ. The curves are displayed for critical density $s_{\rm crit} = 2$ and driving mechanism $b = 0.4$ (the driving mechanism is associated with the supersonic turbulence).

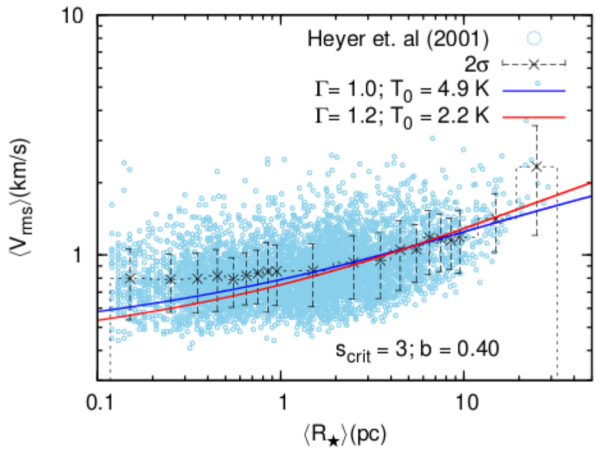

Figure 4. Similar to Figure 3 but with $s_{\rm crit} = 3$.

with $V_0 \sim 1\,{\rm km s^{-1}}$ in the range $\sim 1 - 30\,{\rm pc}$.

Regarding the η parameter, there are two different ranges of values discussed in the literature. The former considers that η lies in the range $0.40-0.50$ (see Hennebelle & Chabrier 2008, 2009). The second discussed in Padoan et al. (2016) and using the same data set of Figure (3) yield η in the interval $0.21 - 0.27$. Our results presented in Figures (3–4) reproduce the Larson's law in the range $1 - 30\,{\rm pc}$ with $V_0 = 0.75{\rm kms^{-1}}$ and $0.20 \leq \eta \leq 0.25$. In addition, our model shows good agreement with the data on the scales where Larson's law is not satisfactory (that is, in the range $\sim 0.1 - 1\,{\rm pc}$).

4. Final remarks

The unified scenario proposed by Gribel et al. (2017), and described in the preceding sections, shows that it is possible to consistently describe both CSFR and SFR in the same model. As a consequence, Larson's law, originally treated empirically in literature, arises as a consequence of the formation of large-scale structures of the universe. The star formation is processed from redshift ~ 20 into low mass halos. As the universe evolves, larger mass halos are formed, but the first structures maintain a similar appearance to GCs, that is, star forming regions with radii of parsecs but embedded by minihalos of dark matter with typical masses $\sim 10^6$ to $10^9 M_\odot$ (see in particular equations 7–8).

This paper does not close the question about the existence or not of non-baryonic dark matter in GCs, but provides a strong indication that there is dark matter, in the form of minihalos, around the stars of the GCs. The presence of non-baryonic dark matter in globular clusters has recently been discussed by several authors (see, e.g., Sollima et al. 2016 and Peñarrubia et al. 2017). Our work shows consistency with these analyses so, at least in principle, our model shows physically healthy properties to jointly describe the CSFR and the SFR, which motivates us to analyze in more depth, in future publications, if GCs may be embedded in dark matter minihalos.

Acknowledgements. We thank the Brazilian agency FAPESP for support under thematic project 2014/11156-4. O.D.M. thanks CNPq for partial financial support (grant 303350/2015-6). The authors are grateful to Dr. Heyer for having made available the CO data used in this work.

References

Armandroff, T.E. & Zinn, R. 1988, AJ, 96, 92
Ashman, K.M. & Zepf, S.E. 1992, American Astronomical Society, 181st AAS Meeting, Bulletin of the American Astronomical Society, Vol. 24, 1186
Bromm, V. & Clarke, C.J. 2002, ApJ, 566, L1
Côté, P., Marzke, R.O. & West, M.J. 1998, ApJ, 501, 554
Fall, S.M. & Rees, M.J. 1985, ApJ, 298, 18
Forbes, D.A., Brodie, J.P. & Grillmair, C.J. 1987, AJ, 113, 1652
Freeman, K.C. 2017, Annu. Rev. Astron. Astrophys., 55, 1
Gribel, C., Miranda, O.D. & Vilas-Boas, J.W. 2017, ApJ, 849, 108
Hennebelle, P., & Chabrier, G. 2008, ApJ, 684, 395
Hennebelle, P., & Chabrier, G. 2009, ApJ, 702, 1428
Heyer, M.H., Carpenter, J.M., & Snell, R.L. 2001, ApJ, 551, 852
Hopkins, P.F. 2013, MNRAS, 430, 1880
Katz, H. & Ricotti M. 2014, MNRAS, 444, 2377
Larson, R.B. 1981, MNRAS, 194, 809
Padoan, P., Juvela, M., Pan, L., Haugbølle, T., & Nordlund, A. 2016, ApJ, 826, 140
Peebles, P.J.E. & Dicke, R.H. 1968, ApJ, 154, 891
Peñarrubia, J., Varri, A.L., Breen, P.G., Ferguson, A.M.N., & Sánchez-Janssen, R. 2017, MNRAS, 471, L31
Schweizer F. 1987, Nearly normal galaxies: From the Planck time to the present; Proceedings of the Eighth Santa Cruz Summer Workshop in Astronomy and Astrophysics, Santa Cruz, CA. New York, Springer-Verlag, 1987, p. 18-25
Sollima, A., Ferraro, F.R., Lovisi, L., Contenta, F., Vesperini, E., Origlia, L., Lapenna, E., Lanzoni, B., Mucciarelli, A., Dalessandro, E., & Pallanca, C. 2016, MNRAS, 462, 1937